UWB-Based Localization in Large Indoor Scenarios: Optimized Placement of Anchor Nodes

STEFANIA MONICA
GIANLUIGI FERRARI, Senior Member, IEEE
University of Parma, Italy

In this paper, we consider the problem of locating a target node (TN) moving along a corridor in a large industrial environment by means of ultrawide band signaling from fixed anchor nodes (ANs) uniformly positioned at the same height on both sides of the corridor. For a representative geometry of a large indoor (industrial) scenario, we formulate an analytical approach to the optimized placement (in terms of internode distance) of ANs using the criterion of minimizing the average mean square error (MSE) in the time-difference-of-arrival-based estimated positions of the TN. Under the assumption of a fixed variance of the range estimation error, we derive a simple closed-form expression for the optimal inter-AN distance in terms of the corridor width and the height of the ANs. The effectiveness of the analytical approach is confirmed by simulations. We also show that the proposed approach allows the MSE in the TN position estimates to reach the Cramer Rao lower bound.

Manuscript received November 11, 2013; revised April 21, 2014, June 27, 2014, September 4, 2014; released for publication September 6, 2014.

DOI. No. 10.1109/TAES.2014.130722.

Refereeing of this contribution was handled by S. Marano.

Authors' addresses: WASN Laboratory, Department of Information Engineering, University of Parma, Parco Area delle Science 181/A, Parma, PR 43124 Italy, E-mail: (stefania.monica@studenti.unipr.it).

I. INTRODUCTION

In recent years, the problem of locating a source in an indoor environment has been widely studied, since it has various applications in many areas, including military security, home surveillance, and medical supervision [1]. In this paper, we focus on the problem of locating and tracking vehicles and/or people in industrial environments. Wireless sensor networks (WSNs) are a promising technology to address this problem because they combine low power and low rate communications with positioning capabilities [2]. In this context, ultrawide band (UWB) signaling holds the promise of good accuracy in ranging because of its high time resolution [3]. Moreover, owing to an inherent robustness against interference and fading and to a significant obstacles penetration capacity, UWB signaling is an attractive option for source location in short-range communication scenarios [4, 5].

Several positioning techniques can be used to locate a target node (TN) through wireless communications. They are usually based on a two-step approach in which certain parameters (such as signal strength, angle of arrival, or time of flight) are first extracted from the signals traveling between the TN and given anchor nodes (ANs) and, then, used to estimate the position of the TN. The use of a time domain-positioning algorithm takes advantage of a feature of UWB signals (namely, their large bandwidth). As a matter of fact, it is known that, when using a time domain-based approach, the accuracy of the position estimate can be improved by increasing the effective bandwidth of the signal [3]. Time domain-based positioning techniques rely on measurements of the time of flight of signals transmitted between pairs of nodes. If all the nodes have a common clock, then each node can determine the time-of-arrival (TOA) of an incoming signal time-stamped by the sender. If the TN is not synchronized with the ANs but there is synchronization among the ANs, then the time-difference-of-arrival (TDOA) technique can be employed. This technique is based on the estimation of the difference between the arrival times of UWB signals traveling between the TN and the reference ANs [1]. In this paper, in order to avoid the synchronization requirement between the TN and ANs, the TDOA approach is used.

Given the range-difference measurements, various methods have been proposed in the literature to compute a location estimate. Iterative methods—such as Taylor series expansion [6], Gauss-Newton, steepest descent, or Levenberg-Marquardt algorithm [7]—require an accurate initial position estimate (which is often not available) and are computationally expensive. Therefore, closed-form solutions (based, for instance, on the least squares principle) have been proposed [8], including the spherical intersection and interpolation methods [9] and the approximate maximum likelihood and two-stage maximum likelihood (TSML) methods [10, 11].

In this paper, we formulate an analytical approach to optimizing the placement of ANs that minimizes the

estimation error of the TN position for large indoor scenarios. This approach can be applied to, for example, indoor localization of automated guided vehicles (AGVs) in industrial environments. The problem of optimal sensor placement for effective distributed processing has been studied in the literature in various contexts [12, 13]. In [14], the plane intersection (PI) method [15] for localization of the TN has been used to optimize ANs placement in a two-dimensional scenario, i.e., when the TN and the ANs are located on the same plane. Here, we generalize this approach to a three-dimensional scenario where the TN moves on the floor along a corridor and the ANs are positioned uniformly on both sides of the corridor at the same height (e.g., at the top of shelves). Using four ANs, it is possible to estimate the TN position by intersecting the major axes of two three-dimensional conics associated with two three-AN subsets. A mathematical framework for optimized placement of ANs is described. Assuming the variance of the range estimation error is constant (the validity of this assumption is discussed in Appendix A), a simple closed-form expression for the optimal inter-AN distance, as a function of the corridor width and the height of the ANs, is derived. Simulation results (with no approximation involved) confirm the effectiveness of the proposed analytical approach to optimized AN placement. Finally, it is shown that the proposed approach (to optimized AN placement) allows the mean square error (MSE) of the TN position estimates to reach the Cramer-Rao lower bound (CRLB).

This paper is organized as follows. In Section II, we describe a general mathematical framework for conic position estimation of a TN using four ANs. In Section III, we apply the framework of Section II to the special case of dynamic position estimation of a TN moving along a straight line in the middle of a corridor, with the ANs positioned uniformly at the same height on both sides of the corridor. A simple closed-form expression for the optimal inter-AN distance is derived. In Section IV, the effectiveness of the proposed analytic approach to optimized AN placement is evaluated by simulations for both linear and nonlinear paths. In Section V, our results and those obtained when using the TSML algorithm [10] are compared, showing that either approach to optimized placement of ANs allows the MSE of the TN position estimates to reach the CRLB. Finally, Section VI concludes the paper.

II. CONIC LOCALIZATION USING FOUR ANS: GENERAL FRAMEWORK

In the remainder of this paper, it is assumed that the TN moves on the floor (e.g., of a warehouse). Without loss of generality, let this plane be given by

$$\mathcal{P}_0 \triangleq \{(x, y, z) \in \mathbb{R}^3 : z = 0\}. \tag{1}$$

According to [15], the minimum number of ANs needed by the PI method to estimate the TN position is five. However, in the considered scenario, one of the coordinates of the TN is known ($z = 0$) so this number reduces to four. Suppose that the position estimate of the TN is obtained by using the four closest ANs that are in line-of-sight (LOS) with the TN. The ANs' coordinates are denoted as follows:

$$\underline{s}_1 = [x_1, y_1, z_1]^T \qquad \underline{s}_2 = [x_2, y_2, z_2]^T$$

$$\underline{s}_3 = [x_3, y_3, z_3]^T \qquad \underline{s}_4 = [x_4, y_4, z_4]^T.$$

In this section, the ANs are supposed to be freely positioned in the space, while in Section III, a particular case (all ANs positioned at the same height) will be considered.

As soon as the TN receives signals from the four ANs, it can localize itself (by either processing the received signals on board or by sending the data to a server that estimates its position). Let $\underline{u} = [x, y, 0]^T$ and $\underline{\hat{u}} = [\hat{x}, \hat{y}, 0]^T$ be the true and estimated coordinates of the TN, respectively. The true range (denoted as r_i) and the estimated range (denoted as $\hat{r}_i$) of the TN from the ith AN ($i \in \{1, 2, 3, 4\}$) can be written respectively as:

$$r_i = ||\underline{u} - \underline{s}_i|| \qquad \hat{r}_i = ||\underline{\hat{u}} - \underline{s}_i||.$$

According to [16], the TOA measurements can be described by an additive noise model, so that the estimated range $\hat{r}_i$ can be expressed as

$$\hat{r}_i = r_i + \nu_i \tag{2}$$

where ν_i is the range error. In [17], it is shown that, with UWB signaling, the range error can be written as follows:

$$\nu_i = \varepsilon_i + \beta$$

where $\varepsilon_i \sim \mathcal{N}(0, \sigma_i^2)$; ε_i is independent of ε_j for $j \neq i$; and β is the synchronization bias (the same for all the ANs).[1] One can thus write

$$\underline{\varepsilon} \sim \mathcal{N}\Big(\underline{0}, \text{diag}\Big(\sigma_1^2, \sigma_2^2, \sigma_3^2, \sigma_4^2\Big)\Big) \tag{3}$$

where $\varepsilon \triangleq [\varepsilon_1, \varepsilon_2, \varepsilon_3, \varepsilon_4]^T$. Denote the estimated and the true range-differences between the first and jth AN, respectively, as:

$$\hat{\Delta}_{1j} \triangleq \hat{r}_j - \hat{r}_1 \qquad \Delta_{1j} \triangleq r_j - r_1 \qquad j \in \{2, 3, 4\}. \tag{4}$$

All other possible range-differences can then be expressed in terms of $\{\hat{\Delta}_{1j}\}$ and $\{\Delta_{1j}\}$. Inserting (2) into the definitions (4) leads to

$$\hat{\Delta}_{1j} = \Delta_{1j} + \varepsilon_{1j} \qquad j \in \{2, 3, 4\} \tag{5}$$

where $\varepsilon_{1j} \triangleq \varepsilon_j - \varepsilon_1$ is the error in the estimated range-difference between the first and jth AN. From (3), it

[1] A similar model, but for a different expression of the range error ν_i, could be derived for other type of wireless communications, such as WiFi.

follows that

$$\mathbb{E}\big[\varepsilon_{1j}\big] = \mathbb{E}\big[\varepsilon_j\big] - \mathbb{E}\big[\varepsilon_1\big] = 0 \qquad j = 2, 3, 4$$
$$\mathbb{E}\big[\varepsilon_{1j}\varepsilon_{1k}\big] = \mathbb{E}\big[\varepsilon_j\varepsilon_k\big] + \mathbb{E}\big[\varepsilon_1^2\big] = \sigma_j^2\delta_{jk} + \sigma_1^2$$
$$j, k = 2, 3, 4$$

where δ_{jk} is the Kronecker symbol and $\mathbb{E}$ is the expectation operator. By defining

$$\underline{\varepsilon}_1 \triangleq [\varepsilon_{12}, \varepsilon_{13}, \varepsilon_{14}]^T \tag{6}$$

it can be concluded that $\underline{\varepsilon}_1 \sim \mathcal{N}(\underline{0}, \underline{\underline{Q}})$, where

$$\underline{\underline{Q}} = \begin{pmatrix} \sigma_1^2 + \sigma_2^2 & \sigma_1^2 & \sigma_1^2 \\ \sigma_1^2 & \sigma_1^2 + \sigma_3^2 & \sigma_1^2 \\ \sigma_1^2 & \sigma_1^2 & \sigma_1^2 + \sigma_4^2 \end{pmatrix}. \tag{7}$$

With the PI method [15], the position estimate is obtained by intersecting planes, with equations depending on the reference ANs. More precisely, two triples of ANs yield two planes, the intersection of which is a line where the TN has to lie. Once the equation of this line is known, it is sufficient to intersect it with the plane $\mathcal{P}_0$ in order to obtain the estimated position of the TN. Considering, for instance, the two triples of ANs given by $\{\underline{s}_1, \underline{s}_2, \underline{s}_3\}$ and $\{\underline{s}_1, \underline{s}_2, \underline{s}_4\}$, the two planes are given by [15]:

$$\begin{aligned}\mathcal{P}^{(12j)} = \Big\{ & (x, y, z) \in \mathbb{R}^3 : \big(x_{21}\hat{\Delta}_{1j} - x_{j1}\hat{\Delta}_{12}\big)x \\ & + \big(y_{21}\hat{\Delta}_{1j} - y_{j1}\hat{\Delta}_{12}\big)y + \big(z_{21}\hat{\Delta}_{1j} - z_{j1}\hat{\Delta}_{12}\big)z \\ & = -\frac{1}{2}\hat{\Delta}_{12}\hat{\Delta}_{1j}\big(\hat{\Delta}_{1j} - \hat{\Delta}_{12}\big) + \frac{1}{2}\big(a_1^2 - a_2^2\big)\hat{\Delta}_{1j} \\ & -\frac{1}{2}\big(a_1^2 - a_j^2\big)\hat{\Delta}_{12}\Big\} \qquad j \in \{3, 4\}\end{aligned}$$

where $x_{j1} \triangleq x_1 - x_j$, $y_{j1} \triangleq y_1 - y_j$, $z_{j1} \triangleq z_1 - z_j$, and $a_j^2 \triangleq x_j^2 + y_j^2 + z_j^2$, with $j \in \{1, 2, 3, 4\}$.

Since it is assumed that the TN moves on the plane $\mathcal{P}_0$ defined in (1), it can thus be concluded that the vector

$$\underline{\hat{u}}_{[1,2]} \triangleq [\hat{x}, \hat{y}]^T$$

of the estimated x and y coordinates of the TN has to satisfy the following system of equations:

$$\underline{\underline{\hat{A}}}\,\underline{\hat{u}}_{[1,2]} = \underline{\hat{b}} \tag{8}$$

where

$$\underline{\underline{\hat{A}}} = \begin{pmatrix} x_{21}\hat{\Delta}_{13} - x_{31}\hat{\Delta}_{12} & y_{21}\hat{\Delta}_{13} - y_{31}\hat{\Delta}_{12} \\ x_{21}\hat{\Delta}_{14} - x_{41}\hat{\Delta}_{12} & y_{21}\hat{\Delta}_{14} - y_{41}\hat{\Delta}_{12} \end{pmatrix} \tag{9}$$

and

$$\underline{\hat{b}} = \frac{1}{2}\begin{pmatrix} \hat{\Delta}_{12}\hat{\Delta}_{13}\big(\hat{\Delta}_{12} - \hat{\Delta}_{13}\big) + \big(a_1^2 - a_2^2\big)\hat{\Delta}_{13} - \big(a_1^2 - a_3^2\big)\hat{\Delta}_{12} \\ \hat{\Delta}_{12}\hat{\Delta}_{14}\big(\hat{\Delta}_{12} - \hat{\Delta}_{14}\big) + \big(a_1^2 - a_2^2\big)\hat{\Delta}_{14} - \big(a_1^2 - a_4^2\big)\hat{\Delta}_{12} \end{pmatrix}. \tag{10}$$

Similarly, the actual coordinates $\underline{u}_{[1,2]} = [x, y]^T$ of the TN on $\mathcal{P}_0$ would satisfy the following system of equations:

$$\underline{\underline{A}}\,\underline{u}_{[1,2]} = \underline{b} \tag{11}$$

where $\underline{\underline{A}}$ and $\underline{b}$ are obtained from $\underline{\underline{\hat{A}}}$ and $\underline{\hat{b}}$ by substituting the estimated range-differences $\{\hat{\Delta}_{1j}\}$ with the true ones $\{\Delta_{1j}\}$.

From (5), one can write

$$\underline{\underline{\hat{A}}} = \underline{\underline{A}} + \underline{\underline{E}} \qquad \underline{\hat{b}} = \underline{b} + \underline{e_b} \tag{12}$$

where

$$\underline{\underline{E}} \triangleq \begin{pmatrix} x_{21}\varepsilon_{13} - x_{31}\varepsilon_{12} & y_{21}\varepsilon_{13} - y_{31}\varepsilon_{12} \\ x_{21}\varepsilon_{14} - x_{41}\varepsilon_{12} & y_{21}\varepsilon_{14} - y_{41}\varepsilon_{12} \end{pmatrix} \tag{13}$$

and, for $i \in \{1, 2\}$,

$$\begin{aligned}\big[\underline{e_b}\big]_i \triangleq & \frac{1}{2}\varepsilon_{1i+2}\big[\Delta_{12}^2 - 2\Delta_{12}\Delta_{1i+2} + a_1^2 - a_2^2\big] \\ & -\frac{1}{2}\varepsilon_{12}\big[\Delta_{1i+2}^2 - 2\Delta_{12}\Delta_{1i+2} + a_1^2 - a_{i+2}^2\big] \\ & +\frac{1}{2}\varepsilon_{12}\varepsilon_{1i+2}\big[2\Delta_{12} - 2\Delta_{1i+2}\big] + \varepsilon_{12}^2\Delta_{1i+2} \\ & +\varepsilon_{1i+2}^2\Delta_{12} + \varepsilon_{12}\varepsilon_{1i+2}(\varepsilon_{12} - \varepsilon_{1i+2})\end{aligned} \tag{14}$$

Assuming that the components of vector $\underline{\varepsilon}_1$ defined in (6) are small (which is realistic with UWB signaling), a good approximation of $\underline{e_b}$ can be obtained by omitting nonlinear perturbations in (14), namely nonlinear products of elements of $\underline{\varepsilon}_1$. As will be shown in Section IV, this assumption results in a localization performance degradation. Therefore, it can be stated that

$$\underline{\hat{b}} \simeq \underline{b} + \underline{\varepsilon_b} \tag{15}$$

where the ith component of $\underline{\varepsilon_b}$ is

$$\begin{aligned}\big[\underline{\varepsilon_b}\big]_i = \frac{1}{2}\big(\varepsilon_{1i+2}\big[\Delta_{12}^2 - 2\Delta_{12}\Delta_{1i+2} + a_1^2 - a_2^2\big] + \\ -\varepsilon_{12}\big[\Delta_{1i+2}^2 - 2\Delta_{12}\Delta_{1i+2} + a_1^2 - a_{i+2}^2\big]\big).\end{aligned} \tag{16}$$

Define

$$\underline{\psi} \triangleq \underline{\hat{b}} - \underline{\underline{\hat{A}}}\,\underline{u}_{[1,2]} = \underline{\underline{\hat{A}}}\,\underline{e} \tag{17}$$

where $\underline{e} \triangleq \underline{\hat{u}}_{[1,2]} - \underline{u}_{[1,2]}$ is the difference between the true position of the TN on $\mathcal{P}_0$ and its estimated position, i.e., $\underline{e}$ is the position estimation error. Using (12) and (15), (17) can be written as

$$\underline{\psi} \simeq \underline{b} + \underline{\varepsilon_b} - \Big(\underline{\underline{A}} + \underline{\underline{E}}\Big)\,\underline{u}_{[1,2]} = \underline{\varepsilon_b} - \underline{\underline{E}}\,\underline{u}_{[1,2]} \tag{18}$$

where the last equality follows from (11). Substituting (13) and (16) into (18), the ith component of the vector $\underline{\psi}$

can be approximated as follows:

$$\begin{aligned}\psi_i \simeq\ & \frac{1}{2}\Big[\varepsilon_{1i+2}\left(\Delta_{12}^2 - 2\Delta_{12}\Delta_{1i+2}\right)\\ & \times \varepsilon_{12}\left(\Delta_{1i+2}^2 - 2\Delta_{12}\Delta_{1i+2}\right)\Big]\\ & + \frac{1}{2}\varepsilon_{1i+2}\left(a_1^2 - a_2^2 - 2x_{21}x - 2y_{21}y\right)\\ & - \frac{1}{2}\varepsilon_{12}\left(a_1^2 - a_{i+2}^2 - 2x_{i+21}x - 2y_{i+21}y\right)\\ =\ & \frac{1}{2}\Big[\varepsilon_{1i+2}\left(\Delta_{12}^2 - 2\Delta_{12}\Delta_{1i+2}\right)\\ & - \varepsilon_{12}\left(\Delta_{1i+2}^2 - 2\Delta_{12}\Delta_{1i+2}\right)\Big]\\ & + \frac{1}{2}\varepsilon_{1i+2}\left(r_1^2 - r_2^2\right) - \frac{1}{2}\varepsilon_{12}\left(r_1^2 - r_{i+2}^2\right) \quad i = 1, 2.\end{aligned}$$

Substituting (4) into the previous equation and after some manipulation, one obtains the following approximate expressions for the elements of vector $\underline{\psi}$:

$$\begin{aligned}\psi_1 &\simeq \varepsilon_{13}\, r_3\,(r_1 - r_2) - \varepsilon_{12}\, r_2\,(r_1 - r_3)\\ \psi_2 &\simeq \varepsilon_{14}\, r_4\,(r_1 - r_2) - \varepsilon_{12}\, r_2\,(r_1 - r_4).\end{aligned}$$

Using (4) and (6), the above equations can be written as $\underline{\psi} \simeq \underline{\underline{R}}\,\underline{\varepsilon}_1$, where

$$\underline{\underline{R}} \triangleq \begin{pmatrix} r_2\Delta_{13} & -r_3\Delta_{12} & 0\\ r_2\Delta_{14} & 0 & -r_4\Delta_{12}\end{pmatrix}. \tag{19}$$

Since $\mathbb{E}[\underline{\varepsilon}_1] = \underline{0}$, it follows that $\mathbb{E}[\underline{\psi}] = \underline{0}$ and the covariance matrix of $\underline{\psi}$ is

$$\underline{\underline{\Psi}} \triangleq \mathbb{E}\left[\underline{\psi}\,\underline{\psi}^T\right] \simeq \underline{\underline{R}}\,\mathbb{E}\left[\underline{\varepsilon}_1\underline{\varepsilon}_1^T\right]\underline{\underline{R}}^T = \underline{\underline{R}}\,\underline{\underline{Q}}\,\underline{\underline{R}}^T$$

where $\underline{\underline{Q}}$ is defined in (7).

From (17), assuming that $\det \underline{\underline{\hat{A}}} \neq 0$, the error $\underline{e}$ can thus be written as

$$\underline{\varepsilon} = \underline{\underline{\hat{A}}}^{-1}\,\underline{\psi} \simeq \left(\underline{\underline{A}} + \underline{\underline{E}}\right)^{-1}\,\underline{\underline{R}}\,\underline{\varepsilon}_1.$$

Neglecting, once again, nonlinear perturbations, the error $\underline{e}$ can be approximated as follows:

$$\underline{e} \simeq \underline{\underline{A}}^{-1}\,\underline{\underline{R}}\,\underline{\varepsilon}_1. \tag{20}$$

Therefore, by defining

$$\underline{\underline{B}} \triangleq \underline{\underline{A}}^{-1} \quad \underline{\underline{T}} \triangleq \underline{\underline{B}}\,\underline{\underline{R}} \tag{21}$$

one can finally conclude that $\underline{e} \sim \mathcal{N}\left(\underline{0}, \underline{\underline{C}}\right)$, where

$$\underline{\underline{C}} = \mathrm{cov}(\underline{e}) \simeq \mathbb{E}\left[\underline{\underline{T}}\,\underline{\varepsilon}_1\,\underline{\varepsilon}_1^T\,\underline{\underline{T}}^T\right] = \underline{\underline{T}}\,\underline{\underline{Q}}\,\underline{\underline{T}}^T. \tag{22}$$

The trace of $\underline{\underline{C}}$ is the MSE of the position estimation and can be expressed, as a function of $\underline{\underline{T}}$ and $\underline{\underline{Q}}$, as follows:

$$Tr(\underline{\underline{C}}) \simeq \sigma_1^2 Tr\left(\underline{\underline{T}}\,\underline{\underline{I}}_3\,\underline{\underline{T}}^T\right) + Tr\left(\underline{\underline{T}}\,\mathrm{diag}\left(\left[\sigma_2^2, \sigma_3^2, \sigma_4^2\right]\right)\underline{\underline{T}}^T\right) \tag{23}$$

where $\underline{\underline{I}}_3$ is a 3×3 matrix with all elements equal to 1. Simple matrix calculation leads to the following

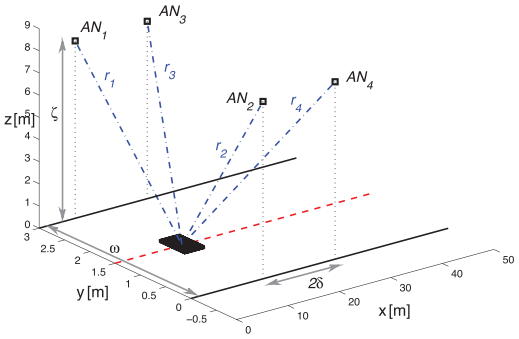

Fig. 1. Corridor in general industrial scenario where TN, represented by black parallelepiped, moves—solid (black) lines on floor represent projections of walls on $\mathcal{P}_0$, thus indicating width of corridor. Four nearest ANs (denoted as AN_1, AN_2, AN_3, AN_4) and their distances $\{r_i\}_{i=1}^4$ (dash-dotted blue lines) from TN are indicated.

approximation:

$$\begin{aligned}Tr\left(\underline{\underline{C}}\right) \simeq \sigma_1^2 &\left[\left(T_{11} + T_{12} + T_{13}\right)^2 + \left(T_{21} + T_{22} + T_{23}\right)^2\right]\\ &+ \sigma_2^2\left(T_{11}^2 + T_{21}^2\right) + \sigma_3^2\left(T_{12}^2 + T_{22}^2\right)\\ &+ \sigma_4^2\left(T_{13}^2 + T_{23}^2\right).\end{aligned} \tag{24}$$

In Section III, $Tr\left(\underline{\underline{C}}\right)$ will be explicitly calculated under certain assumptions, and optimized placement of ANs will be performed by the minimization of a proper function of $Tr\left(\underline{\underline{C}}\right)$

III. AN APPLICATION: DYNAMIC POSITION ESTIMATION WITH TN MOVING ALONG A STRAIGHT LINE AND ANs UNIFORMLY POSITIONED AT THE SAME HEIGHT

Suppose that the TN moves along a straight line[2] in the middle of a corridor of width ω, as shown in Fig. 1 so that its position at time t can be expressed as

$$\underline{u}(t) = \left[x(t), \frac{\omega}{2}, 0\right]^T.$$

We assume that the ANs are alternately positioned on the two sides of the corridor and that they are regularly spaced—this is realistic from an installation perspective for large indoor (e.g., industrial) scenarios. In particular, as shown in Fig. 1, we denote as 2δ the distance between two consecutive ANs on the same side of the corridor along the x–axis (so that δ is the difference in x–coordinate between two consecutive ANs on opposite sides of the corridor). Finally, we also assume that all the ANs are placed at the same height $\zeta \geq 0$, i.e., on the same plane (such as the ceiling of the warehouse) parallel to $\mathcal{P}_0$ (on which the TN moves), given by

[2] In Section IV, it will be shown that the proposed optimized placement strategy provides accurate/satisfactory position estimates even if the TN follows a linear path not in the middle of the corridor/a nonlinear path.

$\mathcal{P}_\zeta \triangleq \{(x, y, z) \in \mathbb{R}^3 : z = \zeta\}$.[3] The above assumptions, which may appear very stringent, are realistic in several industrial scenarios, where shelving units identify straight corridors, along which TNs (e.g., AGVs) move.

As the TN moves along its trajectory, the TN dynamically selects the four closest ANs in LOS to estimate its position, and thus, the framework outlined in Section II can be applied. But for an initial transitory (when $0 \le x(t) \le \delta$) and for the end of the corridor, the considered AN configuration along the corridor is periodic. We remark that the estimation strategy does not change at the beginning and at the end of the corridor, as the four nearest ANs are used. The only difference consists in a different configuration on the ANs with respect to the TN. Therefore, without loss of generality we restrict our attention to the interval $\delta \le x(t) \le 2\delta$, for which the coordinates of the four nearest ANs are given by

$$\underline{s}_1 = [0, 0, \zeta]^T \qquad \underline{s}_2 = [\delta, \omega, \zeta]^T$$
$$\underline{s}_3 = [2\delta, 0, \zeta]^T \qquad \underline{s}_4 = [3\delta, \omega, \zeta]^T.$$

If $\zeta = 0$, then all the ANs are located on the same plane where the TN lies, and this scenario reduces to the one considered in [14].

Given the width ω of the corridor and the height ζ of the ANs, our goal is first to compute $Tr\left(\underline{\underline{C}}\right)$ and then to find the distance δ^* that minimizes a proper function of it. In order to determine an expression for $\underline{\underline{C}}$, explicit expressions of the distances between the TN and the ANs are needed.

Denoting the position of the TN at a given instant as $[\bar{x}, \omega/2, 0]^T$, where $\delta \le \bar{x} \le 2\delta$, one can write:

$$\begin{aligned} r_1^2 &= \bar{x}^2 + \left(\frac{\omega}{2}\right)^2 + \zeta^2 \\ r_2^2 &= (\delta - \bar{x})^2 + \left(\frac{\omega}{2}\right)^2 + \zeta^2 \\ r_3^2 &= (2\delta - \bar{x})^2 + \left(\frac{\omega}{2}\right)^2 + \zeta^2 \\ r_4^2 &= (3\delta - \bar{x})^2 + \left(\frac{\omega}{2}\right)^2 + \zeta^2. \end{aligned} \tag{25}$$

Define[4]

$$\eta^2 \triangleq 4\left[\left(\frac{\omega}{2}\right)^2 + \zeta^2\right]. \tag{26}$$

Substituting (26) into (25) gives:

$$\begin{aligned} r_1 &= \frac{\eta}{2}\sqrt{1+\left(\frac{2\bar{x}}{\eta}\right)^2} & r_2 &= \frac{\eta}{2}\sqrt{1+\left(\frac{2(\delta-\bar{x})}{\eta}\right)^2} \\ r_3 &= \frac{\eta}{2}\sqrt{1+\left(\frac{2(2\delta-\bar{x})}{\eta}\right)^2} & r_4 &= \frac{\eta}{2}\sqrt{1+\left(\frac{2(3\delta-\bar{x})}{\eta}\right)^2}. \end{aligned} \tag{27}$$

If $\eta > 4\delta$, then (since $\delta \le \bar{x} \le 2\delta$) the second-order Taylor series expansion

$$\sqrt{1+\chi^2} = 1 + \chi^2/2 + o\left(\chi^4\right)$$

can be applied to (27), which gives

$$\begin{aligned} r_1 &\simeq \frac{\eta}{2} + \frac{\bar{x}^2}{\eta} & r_2 &\simeq \frac{\eta}{2} + \frac{(\delta-\bar{x})^2}{\eta} \\ r_3 &\simeq \frac{\eta}{2} + \frac{(2\delta-\bar{x})^2}{\eta} & r_4 &\simeq \frac{\eta}{2} + \frac{(3\delta-\bar{x})^2}{\eta}. \end{aligned} \tag{28}$$

Note that the approximate expressions (28) are more accurate for larger η (i.e., larger ω and/or ζ) which corresponds to large indoor scenarios, one of our basic assumptions. According to (26), the condition $\eta > 4\delta$ can be written as

$$\delta < \frac{1}{2}\sqrt{(\omega/2)^2 + \zeta^2}. \tag{29}$$

Therefore, the upper bound for δ increases as the width ω of the corridor and/or the height ζ of the ANs increase.

Substituting (28) into (4) gives:[5]

$$\Delta_{12} \simeq \frac{\delta(\delta - 2\bar{x})}{\eta}\Delta_{13} \simeq \frac{4\delta(\delta-\bar{x})}{\eta}\Delta_{14} \simeq \frac{\delta(9\delta - 6\bar{x})}{\eta} \tag{30}$$

Using (30) and (9), the following approximate expression of $\underline{\underline{A}}$ can be derived:

$$\underline{\underline{A}} \simeq \begin{pmatrix} -2\dfrac{\delta^3}{\eta} & -4\dfrac{\delta(\delta-\bar{x})\omega}{\eta} \\ -6\dfrac{\delta^3}{\eta} & -4\dfrac{\delta(2\delta-\bar{x})\omega}{\eta} \end{pmatrix} \tag{31}$$

so that

$$\det \underline{\underline{A}} \simeq -8\omega\frac{\delta^4}{\eta^2}(\delta - 2\bar{x}).$$

Since $\delta \le \bar{x} \le 2\delta$, it can be concluded that $\det \underline{\underline{A}} > 0$ and, therefore, the matrix $\underline{\underline{B}}$ (21) and the error $\underline{e}$ (20) are well defined.

Before calculating the covariance matrix $\underline{\underline{C}}$ of $\underline{e}$, an explicit expression of $\underline{\underline{T}}$ (and, therefore, of $\underline{\underline{B}}$ and $\underline{\underline{R}}$) is needed. From (31), it follows that

$$\underline{\underline{B}} \simeq \frac{1}{\delta - 2\bar{x}}\begin{pmatrix} \dfrac{\eta}{2\delta^3}(2\delta-\bar{x}) & -\dfrac{\eta}{2\delta^3}(\delta-\bar{x}) \\ -\dfrac{3\eta}{4\delta\omega} & \dfrac{\eta}{4\delta\omega} \end{pmatrix}. \tag{32}$$

[3] It can be shown that, without knowing that the TN moves on a specific plane, the assumption of all ANs located on the same plane would not lead to a unique solution for the TN location problem.

[4] Note that η in (26) reduces to the width of the corridor if $\zeta = 0$.

[5] The quantities in (30) are equal to the ones found in [14], where η is the width of the corridor (because $\zeta = 0$ in [14]).

From (19), using (28) and (30), the entries of $\underline{\underline{R}}$ can be approximated as:

$$\begin{aligned}
R_{11} &\simeq 4\delta(\delta-\bar{x})\left[\frac{1}{2}+\frac{(\delta-\bar{x})^2}{\eta^2}\right]\\
R_{12} &\simeq -\delta(\delta-2\bar{x})\left[\frac{1}{2}+\frac{(2\delta-\bar{x})^2}{\eta^2}\right]\\
R_{21} &\simeq 3\delta(3\delta-2\bar{x})\left[\frac{1}{2}+\frac{(\delta-\bar{x})^2}{\eta^2}\right]\\
R_{23} &\simeq -\delta(\delta-2\bar{x})\left[\frac{1}{2}+\frac{(3\delta-\bar{x})^2}{\eta^2}\right].
\end{aligned} \tag{33}$$

The entries of matrix $\underline{\underline{T}}$ defined in (21) can finally be calculated:

$$\begin{aligned}
T_{11} &= B_{11}R_{11}+B_{12}R_{21} \simeq -\frac{\eta}{2\delta^2}(\delta-\bar{x})\left[\frac{1}{2}+\frac{(\delta-\bar{x})^2}{\eta^2}\right]\\
T_{12} &= B_{11}R_{12} \simeq -\frac{\eta}{2\delta^2}(2\delta-\bar{x})\left[\frac{1}{2}+\frac{(2\delta-\bar{x})^2}{\eta^2}\right]\\
T_{13} &= B_{12}R_{23} \simeq \frac{\eta}{2\delta^2}(\delta-\bar{x})\left[\frac{1}{2}+\frac{(3\delta-\bar{x})^2}{\eta^2}\right]\\
T_{21} &= B_{21}R_{11}+B_{22}R_{21} \simeq -\frac{3\eta}{4\omega}\left[\frac{1}{2}+\frac{(\delta-\bar{x})^2}{\eta^2}\right]\\
T_{22} &= B_{21}R_{12} \simeq \frac{3\eta}{4\omega}\left[\frac{1}{2}+\frac{(2\delta-\bar{x})^2}{\eta^2}\right]\\
T_{23} &= B_{22}R_{23} \simeq -\frac{\eta}{4\omega}\left[\frac{1}{2}+\frac{(3\delta-\bar{x})^2}{\eta^2}\right].
\end{aligned} \tag{34}$$

Using the above results, it is now possible to calculate $Tr\left(\underline{\underline{C}}\right)$.

In [17], it is shown that σ_i ($i \in \{1,2,3,4\}$) can be approximately modeled as a linear function of the distance between the ith AN and the TN:[6]

$$\sigma_i \simeq 0.01 \cdot r_i + 0.08 \quad [\text{m}]. \tag{35}$$

Since we consider the four ANs nearest to the TN (so that all $\{r_i\}_{i=1}^4$ are similar), it is expected that the standard deviations $\{\sigma_i\}_{i=1}^4$ of the range estimation errors associated with the four closest ANs are similar. In Appendix A, it is shown that the standard deviations $\{\sigma_i\}_{i=1}^4$ can be approximated as constant (for $\bar{x} \in [\delta, 2\delta]$) and equal to each other. In particular, we denote the common value of the standard deviations as σ. In the remainder of this section, we show that the optimal inter-AN distance does not depend on σ. Under the assumption that $\sigma_i \simeq \sigma$ for $1 \le i \le 4$, (7) reduces to

$$\underline{\underline{Q}} \simeq \sigma^2 \begin{pmatrix} 2 & 1 & 1 \\ 1 & 2 & 1 \\ 1 & 1 & 2 \end{pmatrix}.$$

Also, (24) becomes

$$\begin{aligned}
Tr\left(\underline{\underline{C}}\right) \simeq \sigma^2\Big[&\left(T_{11}+T_{12}+T_{13}\right)^2+\left(T_{21}+T_{22}+T_{23}\right)^2\\
&+T_{11}^2+T_{12}^2+T_{13}^2+T_{21}^2+T_{22}^2+T_{23}^2\Big].
\end{aligned} \tag{36}$$

In Appendix B, it is shown that the trace of the covariance matrix $\underline{\underline{C}}$ can be written as

$$Tr\left(\underline{\underline{C}}\right) \simeq \frac{\sigma^2}{4\omega^2\eta^2\delta^4}\sum_{i=0}^{6} C_i \bar{x}^i \tag{37}$$

where the coefficients $\{C_i\}_{i=0}^6$ depend on the position $\bar{x}$ of the TN, η (and, therefore, on the width ω of the corridor and on the height ζ of the ANs), and δ. Explicit expressions of the coefficients $\{C_i\}_{i=0}^6$ are also given in Appendix B.

Because of the geometry of the considered scenario, $Tr\left(\underline{\underline{C}}\right)$ is a periodic function of $\bar{x}$. Therefore, in order to compute its average value, it is sufficient to evaluate it over a period: $\delta \le \bar{x} \le 2\delta$. The average value of $Tr\left(\underline{\underline{C}}\right)$ over $\bar{x}$ is given by:

$$\mu(\delta) \triangleq \frac{1}{\delta}\int_{\delta}^{2\delta} Tr\left(\underline{\underline{C}}\right)\mathrm{d}\bar{x}. \tag{38}$$

In order to optimize the placement of ANs, our strategy consists in finding the inter-AN distance δ that minimizes the average MSE $\mu(\delta)$ of the TN position estimates.

Inserting (37) into (38) and using the explicit expressions of the coefficients in (37) (given in Appendix B), the following expression for $\mu(\delta)$ can be obtained:

$$\begin{aligned}
\mu(\delta) \simeq \frac{\sigma^2}{4\omega^2\eta^2}\Bigg[&4\delta^4+\left(\frac{76}{35}\omega^2+\frac{8}{3}\eta^2\right)\delta^2+\frac{22}{15}\eta^2\omega^2\\
&+\frac{5}{4}\eta^4+\frac{1}{3}\eta^4\omega^2\delta^{-2}\Bigg].
\end{aligned}$$

In order to minimize $\mu(\delta)$, we set its derivative to zero. Observing that

$$\frac{\mathrm{d}\mu}{\mathrm{d}\delta} \simeq \frac{\sigma^2}{\omega^2\eta^2}\left(4\delta^3+\left(\frac{38}{35}\omega^2+\frac{4}{3}\eta^2\right)\delta-\frac{1}{6}\eta^4\omega^2\delta^{-3}\right) \tag{39}$$

if we multiply both sides of the equation by $\delta^3/(4\eta^6)$ and define

$$\beta \triangleq \delta^2/\eta^2 \tag{40}$$

it can be concluded that

$$\frac{\mathrm{d}\mu}{\mathrm{d}\delta} = 0 \;\tilde{\Leftrightarrow}\; g(\beta) \triangleq \beta^3+\left(\frac{19}{70}\lambda^2+\frac{1}{3}\right)\beta^2-\frac{1}{24}\lambda^2 = 0 \tag{41}$$

where $\lambda = \omega/\eta$ and the approximate $\sim$ sign on top of the equivalence is due to the fact that the expression on the

[6] The numerical values in (35) were derived in [17] using Channel Model 3 described in [18] and the energy detection receiver presented in [19], which is composed of a band-pass filter followed by a square-law device and an integrator, in which the integration interval is set equal to $T_s = 1$ s. We assume that the same energy detector receiver is used here.

right-hand side of (39) is approximate. It will be shown that all the approximations do not significantly degrade the accuracy of the estimate of the optimal value for δ. The cubic equation on the right hand side of (41) can be solved analytically. More precisely, defining $b \triangleq 19\lambda^2/70 + 1/3$, $d \triangleq -\lambda^2/24$, and $\Lambda \triangleq d^2/4 + b^3 d/27$, one explicit root of (41) is

$$\beta_1 = \sqrt[3]{-\frac{b^3}{27} - \frac{d}{2} + \sqrt{\Lambda}} + \sqrt[3]{-\frac{b^3}{27} - \frac{d}{2} - \sqrt{\Lambda}} - \frac{b}{3}. \tag{42}$$

If $\Lambda > 0$, then β_1 is the only real solution of (41) and, therefore, the correct solution is $\beta^* = \beta_1$. If $\Lambda \leq 0$, then all the solutions of (41) are real. In this case, one can calculate the remaining two solutions β_2 and β_3 of (41) as the solutions of the quadratic equation obtained by dividing $g(\beta)$ by $\beta - \beta_1$, and then select β^* from $\{\beta_1, \beta_2, \beta_3\}$. Note that, by definition (40), β^* has to be positive, and, for the considered problem, only one of the solutions $\{\beta_i\}_{i=1}^3$ is positive. The reason for the latter is that the derivative of $g(\beta)$ is $\beta(3\beta + 2b)$ which (since $b > 0$) is always positive for $\beta > 0$ and since $g(0) = d < 0$, so $g(\beta) = 0$ has only one positive solution. Therefore, we can conclude that $\beta^* = \max\{\beta_1, \beta_2, \beta_3\}$.

Finally, from (40) the optimal value for δ (denoted as δ^*) is given by

$$\delta^* = \sqrt{\beta^*}\eta = \sqrt{\beta^*(\omega^2 + 4\zeta^2)}. \tag{43}$$

As observed in [14], if $\zeta = 0$, i.e., the ANs are located on the same plane where the TN moves, the optimal value δ^* is approximately half of the width of the corridor ($\delta^* \simeq w/2$).

IV. SIMULATION-BASED VALIDATION

The closed-form expression for δ^* (43) is now validated by simulations. The localization performance is evaluated in terms of root mean square error (RMSE), which is defined as follows:

$$\text{RMSE} \triangleq \sqrt{\mathbb{E}[(\hat{x} - x)^2] + \mathbb{E}[(\hat{y} - y)^2]}.$$

Besides considering the scenario presented in Section III (where the TN moves along a straight line in the middle of a corridor of width ω), we will also consider other paths, namely, linear paths not in the middle of the corridor (identified by a parameter c described later) and a nonlinear path. More precisely, if the AGV moves along a straight line parallel to the walls of the corridor, its position at time t can be expressed as $[x(t), c\ \omega, 0]^T$, where $c \in (0,1)$. The case in which the linear path is exactly in the middle of the corridor corresponds to $c = 0.5$. It will be shown by simulations that the optimized AN placement for $c = 0.5$ is also "effective" for other values of c.

Simulation results are obtained by means of a Matlab simulator, based on the one described in [17], in which the standard IEEE 802.15.4a is implemented, using Channel Model 3 described in [18] and the energy detection receiver proposed in [19]. We remark that the simulator does not make any simplifying assumption (like those needed in the formulation of the analytical framework).

TABLE I
Optimal Values of δ Predicted by (43) as the Height ζ of the ANs Varies Between 0 and 10 m and the Width ω of the Corridor Varies Between 2 and 5 m

	δ^* (m)			
	$\omega = 2$ m	$\omega = 3$ m	$\omega = 4$ m	$\omega = 5$ m
$\zeta = 0$ m	0.95	1.42	1.89	2.37
$\zeta = 1$ m	1.19	1.61	2.04	2.49
$\zeta = 2$ m	1.60	2.00	2.40	2.80
$\zeta = 3$ m	1.96	2.39	2.80	3.19
$\zeta = 4$ m	2.27	2.76	3.19	3.60
$\zeta = 5$ m	2.56	3.10	3.56	3.99
$\zeta = 6$ m	2.81	3.41	3.91	4.36
$\zeta = 7$ m	3.05	3.70	4.24	4.72
$\zeta = 8$ m	3.27	3.97	4.54	5.05
$\zeta = 9$ m	3.48	4.22	4.83	5.38
$\zeta = 10$ m	3.67	4.46	5.11	5.68

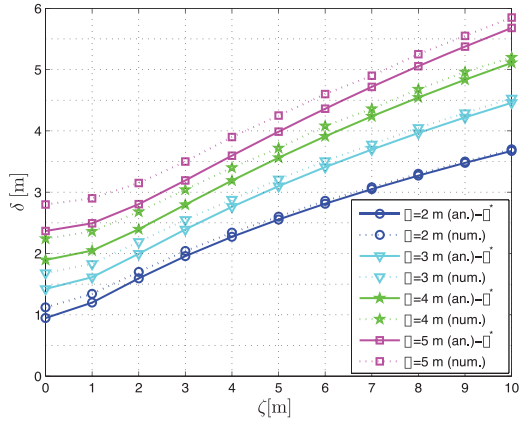

Fig. 2. Optimal inter-AN distance δ^* as function of ζ: values obtained using closed-form expression (43) (solid lines) are compared with values obtained numerically without any approximation (dotted lines). Various values of ω are considered.

Table I shows the optimal values, predicted by (43), of the inter-AN distance, as the width ω of the corridor varies between 2 m and 5 m and the height ζ of the ANs varies between 0 m and 10 m. Observe that the optimal values δ^* do not satisfy the condition (29) behind the approximate expressions (28) for all cases. More precisely, the condition (29) is fulfilled only for small values of ω and large values of ζ. This is consistent with the assumption of large industrial scenarios, where ANs may be attached to the ceiling (which is usually high) and the width of the corridors between shelves is usually kept as small as possible, in order to increase the space dedicated to goods storage.

We remark that, without the Taylor series approximation (28), the values of δ^* could have been evaluated numerically. In Fig. 2, we compare the optimal values δ^* predicted by (43), as a function of ζ, with the values obtained numerically without any approximation—in the latter case, no closed-form

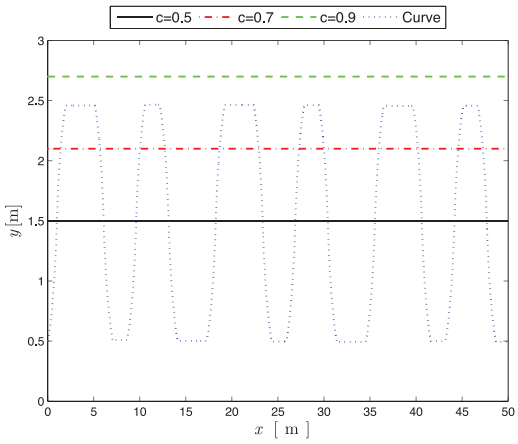

Fig. 3. Considered paths of TN on *xy*-plane.

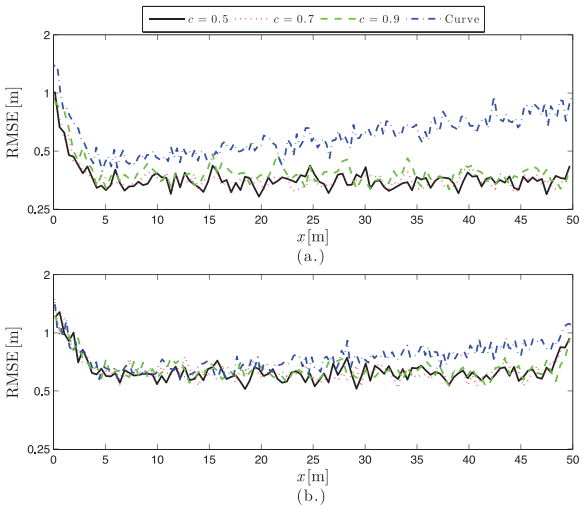

Fig. 4. For each of four paths shown in Fig. 3, RMSE in TN position estimates is shown as function of traveled distance, when: (a.) $\zeta = 5$ m and (b.) $\zeta = 8$ m. In all cases, $\omega = 3$ m and $\delta = \delta^*$.

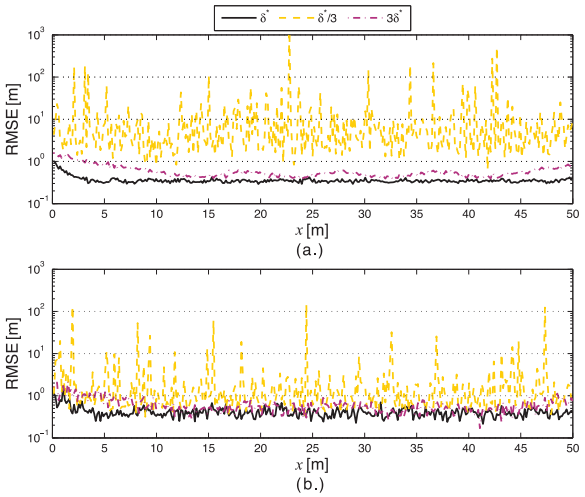

Fig. 5. RMSE in TN position estimates when AGV moves along straight line in middle of corridor ($c = 0.5$) when $\omega = 3$ m: (a.) $\zeta = 5$ m and (b.) $\zeta = 8$ m. In both cases, various values of δ (namely, δ^*, $\delta^*/3$, $3\delta^*$) are considered.

expression can be found. Various values of ω are considered. It can be observed that, whenever the Taylor approximation holds (i.e., large ζ and/or small ω), the values of δ^* predicted by (43) are very accurate. The largest difference between the closed-form solution and the numerical solution is approximately 0.4 m and corresponds to the case where $\omega = 5$ m and $\zeta = 0$ m, which is not a typical industrial scenario. In the remainder of this section, the value δ^* refers to that obtained using (43).

We now investigate the applicability of the optimal inter-AN distance δ^* predicted by (43) (derived under the assumption that the TN moves along a straight line in the *middle* of the corridor) to different paths. We consider a scenario where a TN moves in a 50 m-long corridor with width $\omega = 3$ m. The RMSE in the TN position estimates at each TN position is obtained by averaging the results over 100 realizations. In Fig. 3, four different paths are shown. More precisely, the solid line corresponds to the case where $c = 0.5$ (the AGV moves along the middle line of the corridor); the dash-dotted line corresponds to the case where $c = 0.7$ (the AGV moves along a straight line 0.6 m away from the middle line); the dashed line corresponds to the case where $c = 0.9$ (the AGV moves along a straight line 1.2 m away from the middle line, i.e., 0.3 m from a wall). Finally, the dotted line corresponds to a representative case in which the AGV moves along a curvilinear path.

In Fig. 4, the RMSE in the TN position estimates is shown, as a function of the travelled distance, as the TN moves along each of the four paths for two different values of the height ζ of the ANs: (a.) 5 m and (b.) 8 m. From Table I, the optimal value δ^* is 3.10 m for case (a.) and 3.97 m for case (b.). It can be observed that the use of the optimal value δ^* is "effective" for all three linear paths[7]: the RMSE curves for the three cases are very close to each other. In the case of the nonlinear path, the RMSE curve obtained with δ^* is similar to those of the linear paths for $\zeta = 8$ m (case b.), while it is higher for $\zeta = 5$ m (case a.).

It is now of interest to investigate the effect of a nonoptimal AN placement, i.e., when the actual inter-AN distance δ is not δ^*, on the localization performance. In Fig. 5, we investigate the effect when $\delta \neq \delta^*$ assuming that the AGV moves along a straight line in the middle of the corridor ($c = 0.5$) for (a.) $\zeta = 5$ m and (b.) $\zeta = 8$ m. In both cases, the considered values of δ are δ^*, $\delta^*/3$, and $3\delta^*$. From Fig. 5, it can be observed that, as expected, the lowest RMSE curve is obtained when the optimal value δ^* is used. Also, a smaller value of δ leads to significant peaks in the RMSE curve. On the other hand, increasing the value of δ beyond δ^* has a less significant impact on the RMSE curve.

[7] We remark that, though δ^* is optimal for $c = 0.5$, it may not be optimal for other values of c.

TABLE II
Optimal Values of δ Numerically Evaluated when Using the TSML Method as the Height ζ of the ANs Varies Between 0 and 10 m and the Width ω of the Corridor Varies Between 2 and 5 m

	δ^* (m)			
	$\omega = 2$ m	$\omega = 3$ m	$\omega = 4$ m	$\omega = 5$ m
$\zeta = 0$ m	1.22	1.82	2.43	3.04
$\zeta = 1$ m	1.41	1.98	2.55	3.14
$\zeta = 2$ m	1.74	2.28	2.83	3.39
$\zeta = 3$ m	2.04	2.61	3.15	3.70
$\zeta = 4$ m	2.31	2.91	3.47	4.02
$\zeta = 5$ m	2.55	3.20	3.78	4.34
$\zeta = 6$ m	2.78	3.46	4.07	4.65
$\zeta = 7$ m	2.99	3.71	4.35	4.95
$\zeta = 8$ m	3.18	3.94	4.61	5.23
$\zeta = 9$ m	3.37	4.17	4.87	5.51
$\zeta = 10$ m	3.54	4.38	5.10	5.77

V. COMPARISON BETWEEN THE PI METHOD AND THE TSML METHOD

In this section, we compare the values of δ^* predicted by (43) with the values numerically obtained when using the TSML method [10]. This comparison is meaningful because the TSML method can attain, as shown in [10], the CRLB, but it does not lead to a closed-form expression for δ^*. We also remark that the TSML method involves the solution of a 3 $\times$ 3 system of equations for each position estimate, while the PI method involves the solution of a 2 $\times$ 2 system of equations and is, therefore, more computationally efficient.

Table II shows the optimal values of δ numerically obtained with the TSML method. As in Table I, the width ω of the corridor varies between 2 m and 5 m and the height ζ of the ANs varies between 0 m and 10 m. By comparing the results in Table I with those in Table II, it can be observed that the optimal values for δ are very similar for the two cases (especially for high values of ζ and small values of ω, which correspond to the most practical configurations, as stated in Section IV). Also, the values obtained with the TSML method are very similar to those of the PI method without any approximation, shown in Fig. 2.

In Fig. 6, the MSE is shown as a function of the travelled distance, for both PI and TSML methods, when the TN moves along a corridor with width $\omega = 3$ m. More precisely, Fig. 6 (a.) corresponds to the case in which the TN moves along the middle line of the corridor ($c = 0.5$), while Fig. 6 (b.) corresponds to the case where the TN moves along a straight line near a wall ($c = 0.9$). In both cases, the height of the ANs $\zeta = 5$ m and the inter-AN distance $\delta = \delta^*$. It can be observed that the PI method and the TSML method result in the same localization accuracy. In Fig. 6, the CRLB on the MSE when $\delta = \delta^*$ is also shown. According to [10], the CRLB on the MSE can be expressed as the trace of the matrix $\underline{\underline{G}} \triangleq c^2 \left(\underline{\underline{\Omega}}^T \underline{\underline{Q}}^{-1} \underline{\underline{\Omega}} \right)^{-1}$, where c is the speed of sound

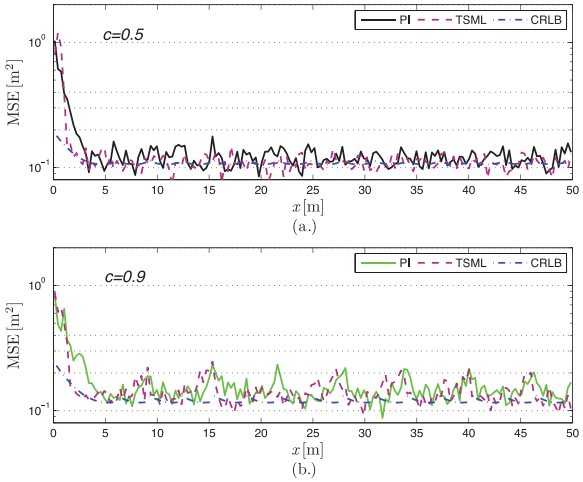

Fig. 6. MSE in TN position estimates for PI method (solid line) and TSML method (dashed line) when TN moves along corridor with $\omega = 3$ m and $\zeta = 5$ m, $\delta = \delta^*$, and (a.) $c = 0.5$ and (b.) $c = 0.9$. Also, CRLB when $\delta = \delta^*$ is plotted.

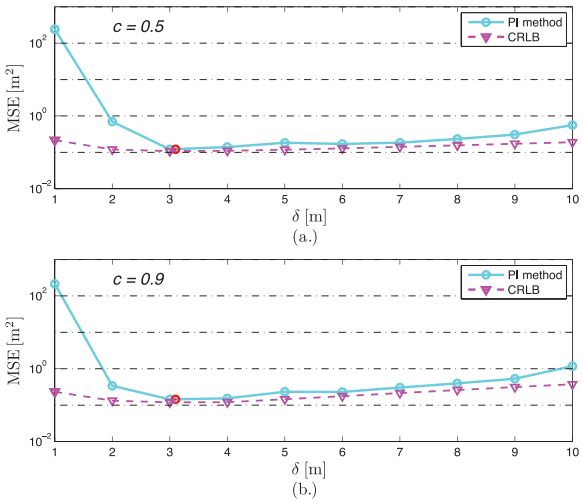

Fig. 7. Average MSE with PI method (solid line) and average CRLB (dashed line), as function of δ, when TN moves along straight line: (a.) in middle of corridor ($c = 0.5$) and (b.) near wall ($c = 0.9$). In both cases, $\omega = 3$ m and $\zeta = 5$ m.

propagation in air, $\underline{\underline{Q}}$ is defined in (7), and $\underline{\underline{\Omega}}$ is the following 3 $\times$ 2 matrix:

$$\underline{\underline{\Omega}} \triangleq \begin{pmatrix} \frac{x_1 - x}{r_1} - \frac{x_2 - x}{r_2} & \frac{y_1 - y}{r_1} - \frac{y_2 - y}{r_2} \\ \frac{x_1 - x}{r_1} - \frac{x_3 - x}{r_3} & \frac{y_1 - y}{r_1} - \frac{y_3 - y}{r_3} \\ \frac{x_1 - x}{r_1} - \frac{x_4 - x}{r_4} & \frac{y_1 - y}{r_1} - \frac{y_4 - y}{r_4} \end{pmatrix}.$$

From Fig. 6, the PI method performs closely to the TSML method and its MSE approaches CRLB (but for border effects). It is of interest to investigate the effect when $\delta \neq \delta^*$. In Fig. 7, the average MSE is shown as a function of δ when the TN moves along a straight line (a.) in the middle of the corridor ($c = 0.5$) and (b.) near a wall ($c = 0.9$). In both cases, the width of the corridor $\omega = 3$ m

and the height of the ANs $\zeta = 5$ m. As expected, the lowest average MSE is reached when $\delta = \delta^*$, the optimal value of δ predicted by (43). For comparison purposes, in Fig. 7 the average CRLB (over the entire path) is also shown as a function of δ. Even though the lowest value of the average CRLB is obtained when $\delta = \delta^*$, it can be observed that the average CRLB has a "milder" dependence on δ.

VI. CONCLUSION

In this work, we have proposed an analytical approach to optimized ANs placement for efficient TDOA UWB-based localization of a TN moving along a corridor in large indoor scenarios. We have imposed the realistic design constraints that the ANs are equally spaced and placed at the same height (e.g., on the ceiling). Assuming that the TN moves along a straight line in the middle of the corridor, we have derived a closed-form expression for the optimal distance between consecutive ANs that minimizes the average MSE of the TN position estimates. The validity of the closed-form expression has been confirmed by simulations, which also show that the proposed placement strategy is also "effective" even when the TN follows other paths different from the linear one in the middle of the corridor. Moreover, we have shown that our approach allows the position estimate accuracy to reach the CRLB.

APPENDIX A

For $\bar{x} \in [\delta, 2\delta]$, it can be easily shown from (28) that

$$\begin{aligned} r_i \in [r_1^{\min}, r_1^{\max}] &\triangleq \left[\frac{\eta}{2} + \frac{\delta^2}{\eta}, \frac{\eta}{2} + \frac{4\delta^2}{\eta}\right] \quad i \in \{1, 4\} \\ r_i \in [r_2^{\min}, r_2^{\max}] &\triangleq \left[\frac{\eta}{2}, \frac{\eta}{2} + \frac{\delta^2}{\eta}\right] \quad i \in \{2, 3\}. \end{aligned} \tag{44}$$

We now want to show that (1) $\{\sigma_i\}_{i=1}^4$ are approximately independent of $\bar{x}$ as the TN moves in the interval of interest and (2) $\sigma_i \simeq \sigma_j$, for $i,j \in \{1, \ldots, 4\}$ and $i \neq j$. This will justify the assumption that $\{\sigma_i\}_{i=1}^4$ are considered approximately equal to a fixed value σ.

Let us consider $\sigma_1(\bar{x})$ (the same result holds due to geometric symmetry for $\sigma_4(\bar{x})$), and observe that since $\sigma_1(\bar{x}) \in [\sigma_1^{\min}, \sigma_1^{\max}] \forall \bar{x} \in [\delta, 2\delta]$, the following inequality holds:

$$|\sigma_1(\bar{x}) - \bar{\sigma}_1| \leq \frac{1}{2}(\sigma_1^{\max} - \sigma_1^{\min}), \tag{45}$$

where $\bar{\sigma}_1 \triangleq (\sigma_1^{\max} + \sigma_1^{\min})/2$. Dividing (45) by $\bar{\sigma}_1$, one obtains

$$\frac{|\sigma_1(\bar{x}) - \bar{\sigma}_1|}{\bar{\sigma}_1} \leq \frac{1}{2}\frac{\sigma_1^{\max} - \sigma_1^{\min}}{\bar{\sigma}_1} \quad \forall \bar{x} \in [\delta, 2\delta] \tag{46}$$

where the ratio on the left-hand side of (46) represents the relative deviation of $\sigma_1(\bar{x})$ ($\forall \bar{x} \in [\delta, 2\delta]$) from its average value $\bar{\sigma}_1$. Observing from (35) and (28) that

$$\begin{aligned} \sigma_1^{\max} &= 0.01\left(\frac{\eta}{2} + \frac{4\delta^2}{\eta}\right) + 0.08 \\ \sigma_1^{\min} &= 0.01\left(\frac{\eta}{2} + \frac{\delta^2}{\eta}\right) + 0.08 \end{aligned} \tag{47}$$

it follows that

$$\frac{\sigma_1^{\max} - \sigma_1^{\min}}{\bar{\sigma}_1} = \frac{6\frac{\delta^2}{\eta}}{\left(\eta + 5\frac{\delta^2}{\eta} + 16\right)} = \frac{6}{\frac{\eta^2}{\delta^2}\left[1 + \frac{16}{\eta}\right] + 5}. \tag{48}$$

For all the scenarios considered in the paper, it can be shown that the values of η and δ^* satisfy

$$\frac{\eta^2}{\delta^2}\left[1 + \frac{16}{\eta}\right] \geq 18. \tag{49}$$

Substituting (48) into (46) and using (49), the following upper bound for the relative deviation of $\sigma_1(\bar{x})$ from $\bar{\sigma}_1$ is obtained:

$$\frac{|\sigma_1(\bar{x}) - \bar{\sigma}_1|}{\bar{\sigma}_1} \leq \frac{1}{2} \cdot \frac{6}{23} = 12.5\% \quad \forall \bar{x} \in [\delta, 2\delta]. \tag{50}$$

Hence, $\sigma_1(\bar{x})$ can be considered as approximately constant as the TN moves, i.e., $\sigma_1(\bar{x}) \simeq \bar{\sigma}_1$. Since r_4 assumes the same range of values as r_1, it can be concluded that $\sigma_4(\bar{x}) \simeq \bar{\sigma}_1 \forall \bar{x} \in [\delta, 2\delta]$.

Let us now consider $\sigma_2(\bar{x})$ (a similar result holds for $\sigma_3(\bar{x})$). Similar to (46), the relative deviation of $\sigma_2(\bar{x})$ from its average value $\bar{\sigma}_2$ is bounded above as follows:

$$\frac{|\sigma_2(\bar{x}) - \bar{\sigma}_2|}{\bar{\sigma}_2} \leq \frac{1}{2}\frac{\sigma_2^{\max} - \sigma_2^{\min}}{\bar{\sigma}_2} \quad \forall \bar{x} \in [\delta, 2\delta] \tag{51}$$

where $\bar{\sigma}_2 \triangleq (\sigma_2^{\max} + \sigma_2^{\min})/2$. Observing from (35) and (28) that

$$\begin{aligned} \sigma_2^{\max} &= 0.01\left(\frac{\eta}{2} + \frac{\delta^2}{\eta}\right) + 0.08 \\ \sigma_2^{\min} &= 0.01\frac{\eta}{2} + 0.08 \end{aligned} \tag{52}$$

it follows that

$$\frac{\sigma_2^{\max} - \sigma_2^{\min}}{\bar{\sigma}_2} = \frac{2\frac{\delta^2}{\eta}}{\left(\eta + \frac{\delta^2}{\eta} + 16\right)} = \frac{2}{\frac{\eta^2}{\delta^2}\left[1 + \frac{16}{\eta}\right] + 1}. \tag{53}$$

Substituting (53) into (51) and using (49) one obtains:

$$\frac{|\sigma_2 - \bar{\sigma}_2|}{\bar{\sigma}_2} \leq \frac{1}{2} \cdot \frac{2}{19} = 5\%. \tag{54}$$

It can thus be concluded that $\sigma_2(\bar{x})$ is approximately constant as the TN moves in the interval of interest, i.e., $\sigma_2(\bar{x}) \simeq \bar{\sigma}_2 \forall \bar{x} \in [\delta, 2\delta]$. Since r_3 assumes the same range of values as r_2, it can also be concluded that $\sigma_3(\bar{x}) \simeq \bar{\sigma}_2 \forall \bar{x} \in [\delta, 2\delta]$.

We now show that the two values $\bar{\sigma}_1$ and $\bar{\sigma}_2$ are very close to each other. Using (47) and (52):

$$\frac{\bar{\sigma}_1}{\bar{\sigma}_2} = \frac{(\sigma_1^{\max} + \sigma_1^{\min})/2}{(\sigma_2^{\max} + \sigma_2^{\min})/2} \tag{55}$$

$$= \frac{0.01\left(\eta + 5\frac{\delta^2}{\eta}\right) + 0.16}{0.01\left(\eta + \frac{\delta^2}{\eta}\right) + 0.16} \tag{56}$$

$$= 1 + \frac{4\frac{\delta^2}{\eta}}{\left(\eta + \frac{\delta^2}{\eta}\right) + 16}. \tag{57}$$

For all the scenarios considered in the paper, it can be shown that the values of η and δ^* satisfy

$$0 \leq \frac{4\frac{\delta^2}{\eta}}{\left(\eta + \frac{\delta^2}{\eta}\right) + 16} \leq 0.2.$$

Using this result in (55) gives

$$1 \leq \frac{\bar{\sigma}_1}{\bar{\sigma}_2} \leq 1.2 \tag{58}$$

i.e.,

$$\bar{\sigma}_1 \simeq \bar{\sigma}_2.$$

Combining the above results, one can assume that $\sigma_i \simeq \sigma, \forall i \in \{1, \ldots, 4\}$, where

$$\sigma = \frac{\bar{\sigma}_1 + \bar{\sigma}_2}{2} = 0.01\left(\frac{\eta}{2} + \frac{3\delta^2}{2\eta}\right) + 0.08.$$

APPENDIX B

The trace of the error covariance matrix defined in (22) is given by (24). From (34), one finds that

$$T_{11} + T_{12} + T_{13} = B_{11}\left(R_{11} + R_{12}\right) + B_{12}\left(R_{21} + R_{23}\right)$$

$$T_{21} + T_{22} + T_{23} = B_{21}\left(R_{11} + R_{12}\right) + B_{22}\left(R_{21} + R_{23}\right).$$

Substituting (32) and (33) into the above equations gives

$$T_{11} + T_{12} + T_{13} \simeq -\frac{(2\delta - \bar{x})\eta}{2\delta^2}\left[\frac{1}{2} + \frac{\bar{x}^2}{\eta^2}\right]$$

$$T_{21} + T_{22} + T_{23} \simeq -\frac{\eta}{4\omega}\left[\frac{1}{2} + \frac{\bar{x}^2}{\eta^2}\right].$$

From the above equations and (34), one obtains:

$$\begin{aligned}
&(T_{11} + T_{12} + T_{13})^2 + T_{11}^2 + T_{12}^2 + T_{13}^2 \\
&\simeq \left\{(\delta - \bar{x})^2\left(\left[\frac{1}{2} + \frac{(\delta - \bar{x})^2}{\eta^2}\right]^2 + \left[\frac{1}{2} + \frac{(3\delta - \bar{x})^2}{\eta^2}\right]^2\right)\right. \\
&\quad \left. + (2\delta - \bar{x})^2\left(\left[\frac{1}{2} + \frac{\bar{x}^2}{\eta^2}\right]^2 + \left[\frac{1}{2} + \frac{(2\delta - \bar{x})^2}{\eta^2}\right]^2\right)\right\} \\
&(T_{21} + T_{22} + T_{23})^2 + T_{21}^2 + T_{22}^2 + T_{23}^2 \\
&\simeq \frac{\eta^2}{16\omega^2}\left\{\left[\frac{1}{2} + \frac{\bar{x}^2}{\eta^2}\right]^2 + 9\left[\frac{1}{2} + \frac{(\delta - \bar{x})^2}{\eta^2}\right]^2\right. \\
&\quad \left. + 9\left[\frac{1}{2} + \frac{(2\delta - \bar{x})^2}{\eta^2}\right]^2 + \left[\frac{1}{2} + \frac{(3\delta - \bar{x})^2}{\eta^2}\right]^2\right\}. \quad (59)
\end{aligned}$$

Finally substituting (59) into (36) and after some manipulation gives (37), where (37), where

$$\begin{aligned}
C_0 &= \frac{5}{2}\delta^2\eta^4\omega^2 + 26\delta^4\eta^2\omega^2 + 146\delta^6\omega^2 \\
&\quad + \frac{5}{4}\delta^4\eta^4 + \frac{27}{2}\delta^6\eta^2 + \frac{117}{2}\delta^8 \\
C_1 &= -\Big(468\delta^5\omega^2 + 60\delta^3\eta^2\omega^2 + 3\delta\eta^4\omega^2 \\
&\quad + 15\delta^5\eta^2 + 108\delta^7\Big) \\
C_2 &= \eta^4\omega^2 + 56\delta^2\eta^2\omega^2 + 606\delta^4\omega^2 + 5\delta^4\eta^2 + 81\delta^6 \\
C_3 &= -\Big(24\delta\eta^2\omega^2 + 408\delta^3\omega^2 + 30\delta^5\Big) \\
C_4 &= 5\delta^4 + 158\delta^2\omega^2 + 4\eta^2\omega^2,\ C_5 = -36\delta\omega^2,\ C_6 = 4\omega^2.
\end{aligned}$$

ACKNOWLEDGMENT

We would like to thank the editor and reviewers, especially reviewer 4, for very detailed comments that significantly improved the quality of this manuscript.

REFERENCES

[1] Gezici, S., and Poor, H. V.
Position estimation via ultra-wide-band signals.
Proceedings of the IEEE, **97**, 2 (Feb. 2009), 386–403.

[2] Zhang, J., Orlik, P. V., Sahinoglu, Z., Molisch, A. F., and Kinney, P.
UWB systems for wireless sensor networks.
Proceedings of the IEEE, **97**, 2 (Feb. 2009), 313–331.

[3] Gezici, S., Zhi, T., Giannakis, G. B., Kobayashi, H., Molisch, A. F., Poor, H. V., and Sahinoglu, Z.
Localization via ultra-wideband radios: a look at positioning aspects for future sensor networks.
IEEE Signal Processing Magazine, **22**, 4 (Jul. 2005), 70–84.

[4] Gungor, V. C., and Hancke, G. P.
Industrial wireless sensor networks: challenges, design principles, and technical approaches.
IEEE Transactions on Industrial Electronics, **56**, 10 (Oct. 2009), 4258–4265.

[5] Sahinoglu, Z., Gezici, S., and Guvenc, I.
Ultra-Wideband Positioning Systems: Theoretical Limits, Ranging Algorithms and Protocols. Cambridge, U.K.: Cambridge University Press, 2008.

[6] Foy, W. H.
Position-location solutions by Taylor-series estimation.
IEEE Transactions on Aerospace and Electronic Systems, **AES-12**, 2 (Mar. 1976), 187–194.

[7] Mensing, C., and Plass, S.
Positioning algorithms for cellular networks using TDOA.
In *Proceedings of the IEEE International Conference on Acoustics, Speech and Signal Processing*, (ICASSP 2006), May 2006, Toulouse, 513–516.

[8] Shen, G., Zetik, R., and Thomä, R. S.
Performance comparison of TOA and TDOA based location estimation algorithms in LOS environment.
In *Proceedings of the 5th workshop on Positioning, Navigation and Communication 2008 (WPNC08)*, Hannover, March 2008, 71–78.

[9] Smith, J. O., and Abel, J. S.
Closed-form least-squares source location estimation from range-difference measurements.
IEEE Transactions on Acoustics, Speech and Signal Processing, **ASSP-35**, 12 (Dec. 1987), 1661–1669.

[10] Chan, Y., and Ho, K. C.
A simple and efficient estimator for hyperbolic location.
IEEE Transactions on Signal Processing, **42**, 8 (Aug. 1994), 1905–1915.

[11] Ho, K. C., Lu, X., and Kovavisaruch, L.
Source localization using TDOA and FDOA measurements in the presence of receiver location errors: analysis and solution.
IEEE Transactions on Signal Processing, **55**, 2 (Feb. 2007), 684–696.

[12] Barrett, S.
Optimizing sensor placement for intruder detection with genetic algorithms.
In *IEEE Intelligence and Security Informatics*, New Brunswick, NJ, May 2007, 185–188.

[13] Krause, A., Leskovec, J., Guestrin, C., Vanbriesen, J., and Faloutsos, C.
Efficient sensor placement optimization for securing large water distribution networks.
Journal of Water Resources Planning and Management, **134**, 6 (Nov. 2008), 516–526.

[14] Monica, S., and Ferrari, G.
Optimized anchors placement: an analytical approach in UWB-based TDOA localization.
In *9th International Wireless Communications and Mobile Computing Conference (IWCMC 2013)*, July 2013, Cagliari, Italy, 982–987.

[15] Schmidt, R. O.
A new approach to geometry of range difference location.
IEEE Transactions on Aerospace and Electronic Systems, **AES-8**, 6 (Nov. 1972), 821–835.

[16] Ho, K. C., and Xu, W.
An accurate algebraic solution for moving source location using TDOA and FDOA measurements.
IEEE Transactions on Signal Processing, **52**, 9 (Sep. 2004), 2453–2463.

[17] Busanelli, S., and Ferrari, G.
Improved ultra wideband-based tracking of twin-receiver automated guided vehicles.
Journal of Integrated Computer-Aided Engineering, **19**, 1 (2012), 3–22.

[18] Molisch, A. F., Cassioli, D., Chong, C., Emami, S., Fort, A., Kannan, B., Karedal, J., Kunisch, J., Schantz, H. G., Siwiak, K., and Win, M. Z.
A comprehensive standardized model for ultrawideband propagation channels.
IEEE Transactions on Antennas and Propagation, **54**, 11 (Nov. 2006), 3151–3166.

[19] Dardari, D., Chong, C. C., and Win, M. Z.
Threshold-based time-of-arrival estimators in UWB dense multipath channels.
IEEE Transactions on Communications, **56**, 8 (Aug. 2008), 1366–1378.

Stefania Monica was born in Parma, Italy, in 1987. She received her Laurea degree (three-year program) and her Laurea Magistrale (two-year program) degree (summa cum laude) in mathematics from the University of Parma in September 2009 and July 2011, respectively. From January 2012, she has been a Ph.D. student at the Department of Information Engineering at the University of Parma, and she is a member of the Wireless Ad-hoc and Sensor Networks Lab (http://wasnlab.tlc.unipr.it/people/monica). Her research interests include UWB technology and localization algorithms. She is corecipient of the best paper award at EvoCOMNET 2013.

Gianluigi Ferrari was born in Parma, Italy, in 1974. He received his Laurea and Ph.D. degrees from the University of Parma, Parma, Italy, in 1998 and 2002, respectively. Since 2002, he has been with the University of Parma, where he currently is an associate professor of telecommunications. He was a visiting researcher at University of Southern California, Los Angeles, CA, in 2000–2001, Carnegie Mellon University, Pittsburgh, PA, in 2002–2004, King Mongkut's Institute of Technology Ladkrabang, Bangkok, Thailand, in 2007, and Université Libre du Bruxelles, Brussels, Belgium, in 2010. Since 2006, he has been the coordinator of the Wireless Ad-hoc and Sensor Networks Lab (http://wasnlab.tlc.unipr.it/) at the Department of Information Engineering. As of today, he has published/accepted more than 200 papers in leading international journals and conferences, 22 book chapters, 9 patents, and 8 books. He edited the book *Sensor Networks: Where Theory Meets Practice* (Springer: 2010). His research interests include wireless ad hoc and sensor networking, adaptive digital signal processing, and communication theory. He participates in several research projects funded by public and private bodies (recovered funds over 1.9 M€). Prof. Ferrari is corecipient of a best student paper award at IWWAN'06; a best paper award at EMERGING'10; the first Body Sensor Network (BSN) contest winner award (as a member of the WASNLab team) held in conjunction with BSN 2011; an award for the outstanding technical contributions at ITST-2011; the best paper award at SENSORNETS 2012; the best paper award at EvoCOMNET 2013; the Best Runner-up Paper Award at BSN 2014; and the Best Conference Paper Award at SoftCOM'14 (Symposium on RFID Technologies and Internet of Things). He acts as a frequent reviewer for many international journals and conferences as well as Technical Program Committee member for many international conferences. He currently serves on the editorial boards of several international journals. He was a guest editor of the 2010 EURASIP JWCN Special Issue on "Dynamic Spectrum Access: From the Concept to the Implementation" and of the 2014 Hindawi IJDSN Special Issue on "Advanced Applications of Wireless Sensor Network Using Sensor Cloud Infrastructure." He is a guest editor of the 2015 Hindawi IJDSN Special Issue on "Wireless Sensor Networks for Structural Health Monitoring." He is an IEEE Senior Member.